Journal of Instrumentation

Estimating the surface backgrounds in PandaX-II WIMP search data

Published by IOP Publishing for Sissa Medialab

Received: *September 1, 2019*
Accepted: *October 3, 2019*
Published: *October 25, 2019*

International Summer School on
Intelligent signal processing for FrontIEr Research and Industry
Huazhong University of Science and Technology, HUST, at Wuhan, China
12–26 May 2019

Estimating the surface backgrounds in PandaX-II WIMP search data

D. Zhang

Department of Physics, University of Maryland
College Park, MD, 20742, U.S.A.

E-mail: danavagor@gmail.com

Abstract: We estimate the contribution of surface backgrounds, the radioactivities from the wall, in the search window of weakly interacting dark matter particles (WIMPs) with data outside of the window in the PandaX-II detector. In the former analysis, the surface backgrounds was suppressed to a negligible level with a strong fiducial volume (FV) cut that only includes data at the detector center. This work uses data with nominal reconstructed radius outside of the detector border, where contributions of other resources are negligible, to represent properties of the surface backgrounds except the horizontal positions. As the horizontal position reconstruction only depends on the ionization signals, the latter property of surface backgrounds is parameterized by data with the same ionization signals as the search window but different scintillation signals. With the behavior of the surface backgrounds outside the FV known, the data close to the wall can be used for the WIMP search.

Keywords: Analysis and statistical methods; Dark Matter detectors (WIMPs, axions, etc.); Noble liquid detectors (scintillation, ionization, double-phase)

https://doi.org/10.1088/1748-0221/14/10/C10039

Contents

2019 JINST 14 C10039

1 Introduction

The weakly interacting massive particle (WIMP) with mass on the level of 100 GeV/c^2 is a leading class of dark matter candidates because it can explain the abundance of dark matter in cosmology [1], and has been predicted by many theoretical models such as the supersymmetric theory [2].

The PandaX-II experiment directly detects WIMP-nucleus scattering with a two-phased xenon time projection chamber (TPC), located at the China Jinping Underground Laboratory (CJPL) [3]. It contains 580 kg liquid xenon (Xe) in the 60×60 cm dodecagonal TPC which collects prompt scintillation photons (S1s) and delayed electroluminescence photons (S2s) by photomultiplier tubes (PMTs). For a physical event, S1s are scintillation signals generated in the liquid phase by the de-excitations of xenon atoms and recombinations of electrons and ions, and S2s are ionization signals generated in the gas phase by the free electrons drifted to the surface in a static electric field and extracted by another stronger electric field. A complete description of the detector can be found in ref. [5].

We study the backgrounds in the low energy region because WIMPs on the order of 100 GeV/c^2 typically generate nuclear recoils (NRs) below 10 keV. As in ref. [4], after applying the WIMP-search cuts, including the quality cuts, S2-S1 cut, boosted decision tree (BDT) cut and fiducial volume (FV) cut (361.5 kg Xe), electron recoils (ERs), accidental backgrounds and neutrons are the dominant backgrounds in the region of interest (ROI). The quality cuts are used to eliminate events with abnormal waveforms. The S2-S1 cut suppresses ER backgrounds because for the same S1, the ionization-to-scintillation (S2-to-S1) ratio is larger for ERs than NRs. The BDT cut is trained to reduce accidental backgrounds. The FV cut suppresses events from electrodes and walls to a negligible level.

If we loose the FV cut, the surface backgrounds become the dominant backgrounds, indistinguishable with the other survived events. Surface events are dominant by β decays of ^{210}Pb in the ^{238}U decay chain in the ROI, which has an energy end-point of 63.5 keV and a half-life of 22.2 y. As discussed in [6], only part of the S2s can be collected in the surface events, which causes a lower S2-to-S1 ratio compared to normal ERs. To date no distinct feature can be used to suppress the surface backgrounds if they appear as candidates.

The properties of surface backgrounds in the ROI can be studied with events outside the ROI. The data with nominal reconstructed positions outside the border of our detector can represent the properties of surface events contribute to the backgrounds because other radioactivities are negligible in these events. An exception of the properties is the radial position uncertainties because the horizontal position reconstruction algorithm and the radial electric field result in asymmetric position uncertainties for events inside and outside the nominal border of our detector. Therefore, the estimation of surface backgrounds is factorized into two parts, one describing the radial position uncertainties and the other including other properties.

Besides the parameters used in the old probability distribution functions (PDFs) of backgrounds, S1 and S2, and the radius of the recoiling events, the vertical position, z, is included in the surface-background PDF. Because the marginal effect of the electric field, the distortion of the field close to the wall, and a non-uniform WIMP-search cut efficiency along z, including the vertical information helps to separate the surface backgrounds and other radioactivities.

In this article, the estimates of the surface-background PDF with the Run10 data outside of the ROI is presented. We validate the result by comparing it to the WIMP search data in the window.

2 Modeling the surface-background distribution

The modeling is done for two different horizontal position reconstruction algorithms separately, which provides us with complementary check. One uses analytical photon acceptance functions (PAF), which is used in our previous work [7], and the other uses simulation-based PAFs, similar to the work in the ref. [8] but with extra customized tuning.

As discussed above, the surface-background PDF is factorized into two independent parts, one for the radius distribution, noted as P_R, and the other for S1, S2 and z, denoted as P_d. To parameterize the former part, data with S1 larger than the ROI but the same S2 are used. We first define the nominal border of our detector, termed as the soft wall, by the median positions of the surface events with different z and azimuth angles. Then, P_R is parameterized as a function of S2 and the distance to the soft wall, r_w. For the latter part, P_d, a data-driven histogram related to S1, S2, and z, is fitted with kernel density estimator (KDE) [9], a statistic tool smoothing out the distribution. The final PDF model is

$$P_{b,\mathrm{wall}}(r_w, \mathrm{S1}, \mathrm{S2}, z) = P_R(r_w, \mathrm{S2}) \times P_d(\mathrm{S2}, \mathrm{S1}, z). \tag{2.1}$$

To find the median radial positions of the surface events, data with S1s from 50 to 500 PE are used, which are outside of the ROI. The surface events in this range are dominant by β decays of ^{210}Pb and ^{210}Bi in the ^{238}U decay chain. With the flat distribution inside the detector is subtracted, the median of the one-dimensional event distribution along radius for different z and azimuth angles is set as the border of our detector. Then, the average on the radius of the soft wall is stretched to be the same as the solid boundary of our TPC (329.7 mm). The original reconstructed positions have all been horizontally stretched 7% and 6% for the analytical and simulation-based PAF algorithm, respectively. The stretched soft walls and the corresponding inward 1 σ fluctuations are shown in figure 1, which indicate the uncertainties in different position reconstruction algorithms.

The equivalence of different position reconstruction algorithms is shown in figure 2, which is determined by requiring the same amount of surviving events with the same cuts. The cuts used,

2019 JINST 14 C10039

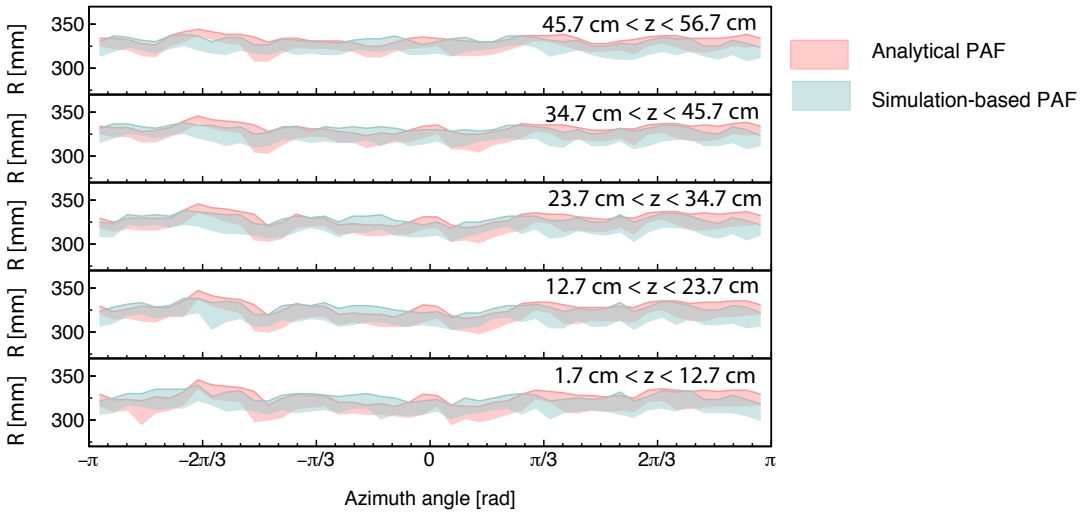

Figure 1. The stretched soft walls and 1 σ inward fluctuation bands with analytical and simulation-based PAF algorithms. The vertical range is bounded from $z = 0$ (the bottom of the TPC) to $z = 60\,\text{cm}$ (the liquid surface).

excluding the radial cut, are the same as mentioned in ref. [4] except for the S1-S2 cut, because the statistics will otherwise be too small. In figure 2, the dashed blue line marks the solid boundary (329.7 mm), and the solid blue line indicates the old FV cut, $R^2 < 7.2 \times 10^4\,\text{mm}^2$ and $1.7\,\text{cm} < z < 56.7\,\text{cm}$, for the former analysis in ref. [4]. The red and green dashed lines are the stretched soft walls averaged over azimuth angle of the analytical and simulation-based PAF algorithms, respectively. The corresponding equivalent radial cut, $r_w < -64.8\,\text{mm}$ / $r_w < -63.9\,\text{mm}$ for the analytical/simulation-based PAF algorithms, is drawn in a dashed line with the same color. In the old FV cut, the dependence on z is neglected, which is included in the parameter r_w in the new FV cuts. The conversion between z and the drifting time, Δt_z, is done with known drifting velocity of free electrons during Run 10, $v_e = 1.7\,\text{mm}/\mu\text{s}$ [4].

After defining the soft walls, $P_R(r_w, \text{S2})$ is built with the same data used in the soft-wall construction, which describe the radius distribution inside the soft wall. The surface-background distributions with different S2s and position reconstruction algorithms are shown in figure 3, where the negative sign of r_w represents inward fluctuation. Larger S2s have smaller fluctuation in the radius, which agrees with our statistical intuition. Due to the asymmetry in the radial position uncertainties, only the events with negative r_w are used to construct P_R.

We use normal functions to fit the inward fluctuation of surface events for different S2s, which means P_R can be modeled as

$$P_R(r_w, \text{S2}) = \frac{1}{\sqrt{2\pi\sigma_r(\text{S2})^2}} \cdot \exp\left(-\frac{r_w^2}{2\sigma_r(\text{S2})^2}\right). \tag{2.2}$$

The fitted standard deviations, σ_r, shown in figure 3 are further parameterized as an analytic function of S2,

$$\sigma_r(\text{S2}) = \frac{1}{p0 - p1 \cdot \log_{10}\text{S2} + p2 \cdot (\log_{10}\text{S2})^2}\,\text{cm}, \quad \text{S2} <= 3000\,\text{PE}, \tag{2.3}$$

2019 JINST 14 C10039

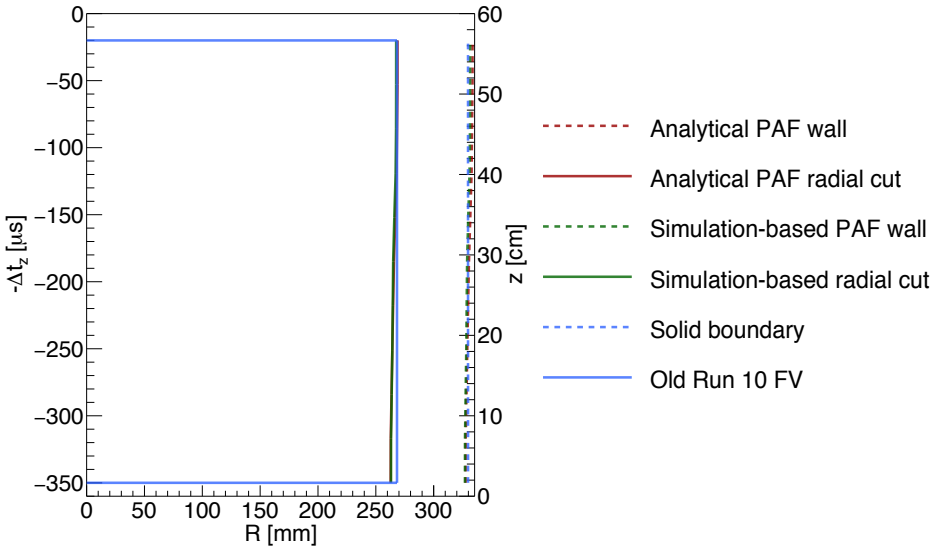

Figure 2. The soft walls and equivalent radial cuts with different position reconstruction algorithms. The radius of the solid boundary (329.7 mm) and the old FV cut used in Run 10 [4] are drawn for reference.

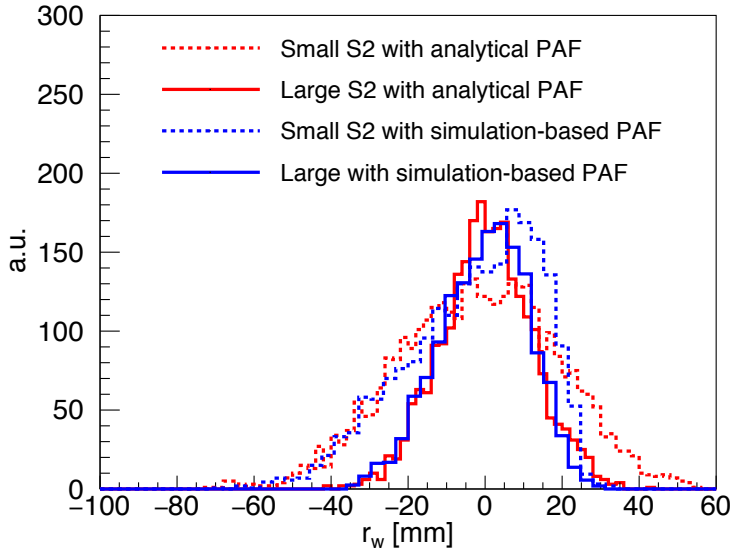

Figure 3. Run 10 surface-background distribution with different S2 ranges and different position reconstruction algorithms with all cuts applied in ref. [4] except the S1-S2 and FV cut. Small S2 is for 200 to 250 PE, and large S2 for 900 to 1100 PE. The inner flat event distribution has been subtracted.

2019 JINST 14 C10039

where $p0$, $p1$ and $p2$ are fitting parameters. The results are $p0$=1.168/0.8002, $p1$=−0.947/−0.6323 and $p2$ = 0.2748/0.2124 for the analytical/simulation-based PAF algorithms. In figure. 4, the points mark the fitting results of the normal distributions, and the lines are further parameterized functions of $\sigma_r(S2)$. When S2 > 3000 PE, the uncertainties in the position reconstruction algorithms start to dominate instead of the statistical uncertainties. In this region, we extend the standard deviation $\sigma_r(3000)$, 8.4 mm/8.5 mm for the analytical or the simulation-based PAF, to the region with larger S2.

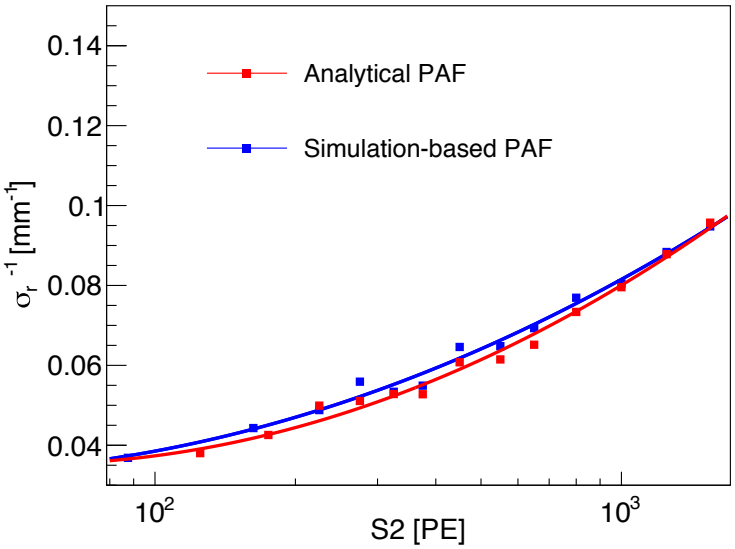

Figure 4. Parameterization of $\sigma_r(S2)$ for different position reconstruction algorithms.

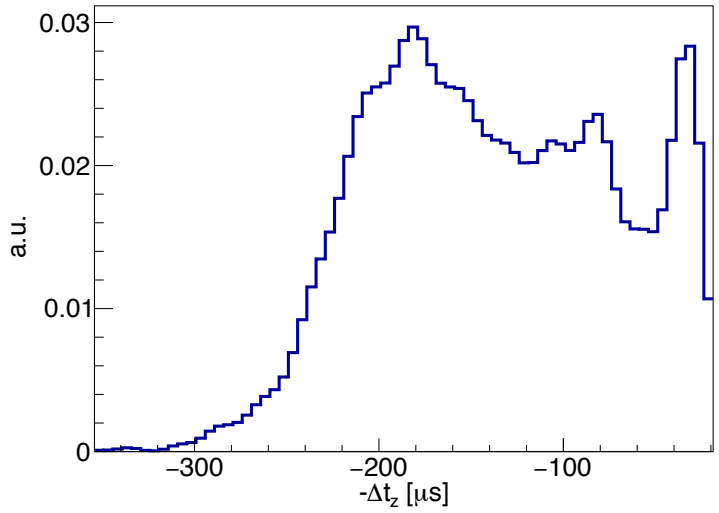

Figure 5. The Δt_z distribution of the Run 10 surface events after applying the WIMP-search cuts excluding the radial cut. Other dimensions are integrated. The drifting time from 20 to 350 μs corresponds to z from 56.7 to 1.7 cm

2019 JINST 14 C10039

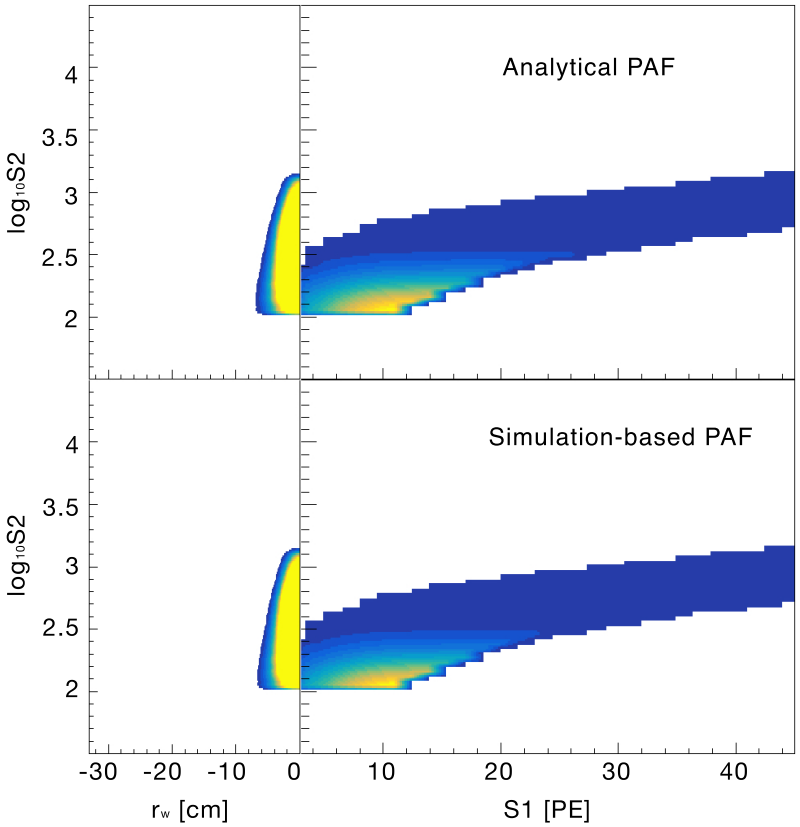

Figure 6. The projections of $P_{b,\text{wall}}$ onto different axises. The top/bottom panel is for the analytical/simulation-based PAF algorithm respectively. The left panels integrate the other two dimensions (S1 and z), and the right panels only integrate events in the corresponding FV.

P_d is constructed independently, to reflect the properties of the surface events other than the radial position uncertainties. The data used to derive P_d are the events survived the WIMP-search cuts in Run 10 except the radius in the FV cut. The events with $r_w > 0$ is used to suppress all the other contributions to a negligible level. We inherit the S1 and S2 from old PDFs which present strong signal discrimination power over ER backgrounds. The z distribution of the surface events is non-trivial. In figure 5, the decrease of surface backgrounds for events with drifting time longer than 200 µs is because of marginal effect of the electric field. The electrons are drifted towards the wall where the radial fraction of the electric field points out, and no S2 will generate. In the data with smaller drifting time, the efficiency of WIMP-search cuts causes irregularity. Therefore, besides r_w and old parameters, z is also included in the new PDF. The original event distribution as a function of S1, S2 and z is smoothed with KDE integrated in Python. Because it is difficult to visualize four-dimensional PDFs according to eq. (2.1), the PDFs are projected as in figure 6.

2019 JINST 14 C10039

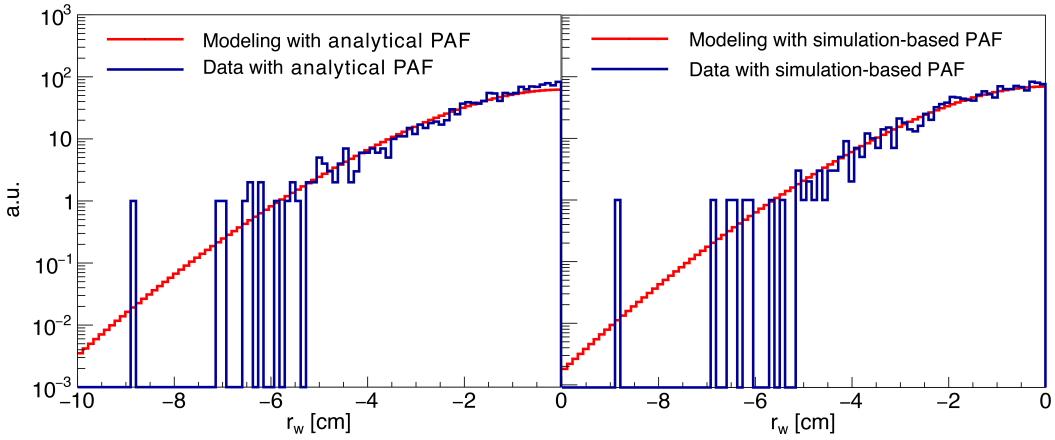

Figure 7. The scaled $P_{b,\text{wall}}$ projected to r_w with the data overlain. The other dimensions are integrated. The scaling factor is the ratio of the integrals for the data and model with r_w from -6 cm to -1 cm. The left and right panel is for the analytical and simulation-based PAF algorithms respectively.

3 Comparison between the model and data

The surface-background PDF is validated by being compared to Run 10 data inside of the ROI. The WIMP search data (blue) and surface-background PDF (red) projected to r_w with all other dimensions integrated are overlain in figure 7, where the PDF is constructed following the procedure mentioned before in the blinding analysis. In this figure, the ratio of the normalized-PDF integral within $-6\,\text{cm} < r_w < -1\,\text{cm}$ to that of the data is used to scaled the PDF. We evaluate the agreement between the PDF and data by scaling with different r_w ranges. There is a 8%/4% uncertainty in the scaling factor for the analytical/simulation-based PAF algorithm.

With the knowledge of the surface-background PDFs, we can estimate contribution of the surface events in the WIMP candidates. As shown in the table 1, even if the numbers of the Run 10 WIMP candidates are different, but with the corresponding surface backgrounds accounted, the results are consistent. The uncertainties are evaluated by ± 2 mm difference in the r_w cut.

Table 1. The comparison of the Run 10 WIMP candidate number (No) with different radial cuts and all other cuts applied using Run 10 data. $\bar{R}$ is the average on the radial cut of different z and azimuth angle in this work. The numbers of surface events are integrated in the corresponding FV with the scaled PDFs.

Data Type	Radius cut	No. of events
Run 10 WIMP candidate (old PAF)	$R < 268.3$ mm	1
Run 10 WIMP candidate (analytical PAF)	$\bar{R} < 264.9$ mm	4
Surface event (analytical PAF)	$\bar{R} < 264.9$ mm	$3.7^{+0.6}_{-0.9}$
Run 10 WIMP candidate (simulation-based PAF)	$\bar{R} < 265.8$ mm	3
Surface event (simulation-based PAF)	$\bar{R} < 265.8$ mm	$2.6^{+0.9}_{-0.4}$

2019 JINST 14 C10039

4 Summary

The surface-background PDF is constructed with Run 10 data outside of the ROI and two different position reconstruction algorithms. The PDF is factorized into two independent parts, one parameterizing the radial position uncertainties of surface events with the data in larger S1 region than the ROI and the other representing distribution in the space of S1, S2, z with the data outside the soft wall.

We assess the surface-background PDF by comparing the projected one-dimensional distribution with respect to r_w with the data in the ROI, especially the part outside the FV but within the border of the detector. The total number of survived surface events is the scaling factor of the normalized one-dimensional PDF that makes the model agree with the data in a certain r_w range. Evaluated by selecting different r_w ranges, the uncertainties in the scaling factors are 8% and 4% in the analytical and simulation-based PAF algorithms respectively.

The suface-background contribution in the corresponding new FV is consistent for both position reconstruction algorithms. With the four-dimensional PDF, we are capable of including more xenon into our analysis in the future.

Acknowledgments

The author is sponsored by the U.S. Department of Energy (DOE) under grant DE-FG02-93ER-40762 for this work. She gratefully acknowledges PandaX Collaboration for providing the data for this analysis, and helpful discussion with Dr. Xiaopeng Zhou from Beihang University and Prof. Jianglai Liu from Shanghai Jiao Tong University. She also thanks PandaX Collaboration for supporting her to attend the summer school, INFIERI2019. She acknowledges the summer school for offering an opportunity to publish this work.

References

[1] Planck collaboration, *Planck 2018 results. VI. Cosmological parameters*, arXiv:1807.06209.

[2] G. Jungman, M. Kamionkowski and K. Griest, *Supersymmetric dark matter*, *Phys. Rept.* **267** (1996) 195 [hep-ph/9506380].

[3] K.J. Kang, J.P. Cheng, Y.H. Chen, Y.J. Li, M.B. Shen, S.Y. Wu et al., *Status and prospects of a deep underground laboratory in China*, *J. Phys. Conf. Ser.* **203** (2010) 012028.

[4] PandaX-II collaboration, *Dark Matter Results From 54-Ton-Day Exposure of PandaX-II Experiment*, *Phys. Rev. Lett.* **119** (2017) 181302 [arXiv:1708.06917].

[5] PandaX collaboration, *Dark Matter Search Results from the Commissioning Run of PandaX-II*, *Phys. Rev.* **D 93** (2016) 122009 [arXiv:1602.06563].

[6] Chang Lee, *Mitigation of Backgrounds for the Large Underground Xenon Dark Matter Experiments*, Ph.D. thesis, Case Western Reserve University (2015).

[7] PandaX-II collaboration, *Dark Matter Results from First 98.7 Days of Data from the PandaX-II Experiment*, *Phys. Rev. Lett.* **117** (2016) 121303 [arXiv:1607.07400].

[8] Jason Philip Brodsky (Darkside-50 Collaboration), *xy Position Reconstruction in Darkside-50*, Ph.D. thesis, Princetion University (2015).

[9] https://pythonhosted.org/PyQt-Fit/mod_kde.html

2019 JINST 14 C10039